Iranian Journal of Materials Forming 7 (1) (2020) 100-115

Online ISSN: 2383-0042

IJMF

Iranian Journal of Materials Forming

Journal Homepage: http://ijmf.shirazu.ac.ir

Multi-response Optimization of the Mechanical and Metallurgical Properties of Al7075-T6 Deposition Process on Al2024-T351 by Friction Surfacing Using RSM and the Desirability Approach

A. Mostafapour[1], M. Moradi[2*], H. Kamali[3], M. Saleh Meiabadi[4] and A. Kaplan[5]

[1] Department of Mechanical Engineering, Faculty of Mechanical Engineering, University of Tabriz, Iran
[2] Department of Mechanical Engineering, Faculty of Engineering, Malayer University, Malayer, Iran
[3] Department of Mechanical Engineering, Faculty of Mechanical Engineering, University of Maragheh, Iran
[4] Department of Mechanical Engineering, École de technologie supérieure, Canada 1100 Notre-Dame West, Montreal, Canada
[5] Department of Engineering Sciences and Mathematics, Lulea University of Technology, Lulea, Sweden

ARTICLE INFO

Article history:

Received 13 December 2019
Revised 17 February 2020
Accepted 7 March 2020

Keywords:

Friction surfacing
Mechanical properties
Aluminum deposition
Optimization
Design of experiments

ABSTRACT

Coating plays a significant role in surface engineering, which leads to the improvement of the mechanical and metallurgical properties of products. It also brings about economic benefits thanks to the cost savings of the improved properties of the surface of a product in particular. Friction surfacing is a relatively new way to create a homogeneous, fine-grained coating with amended resistance to wear and corrosion. In this study, the deposition of Al7075-T6 coating on Al2024-T351 substrates is investigated. Response surface methodology is implemented to study the effects of the rotational speed, axial force, and feed rate on the mechanical properties and microstructure of the specimens. Coating width, coating thickness, ultimate tensile strength, and grain size of coating are considered as the output responses. The input parameters are optimized to attain a wider and thicker coating with higher ultimate tensile strength and of course smaller grain size. Results display the joining of two materials without any porosity at the interface. Moreover, an entirely fine-grained homogeneous microstructure of the deposition is observed. Furthermore, the average grain size of the deposition is diminished by 65% compared to the consumable rod.

1. Introduction

Coating plays a major role in surface engineering and results in the mechanical and metallurgical improvements of products. It also brings about economic benefits thanks to the cost savings associated with the improvement of the surface properties of a product particularly. Friction surfacing (FS) is a solid-state process based on the plastic deformation of a metallic consumable rod to deposit a layer on a substrate. The rotating rod is pressed upon the substrate by the applied axial force, and frictional heating results in a visco-plastic layer at the tip of the rod and in a rising temperature [1]. In addition, compression loading leads to intermediate penetration process and thus developing a metallic joint between the plasticized materials and the substrate. Interfacial friction and plastic deformation are the only thermal sources, in friction surfacing, which allow the processing of materials below the melting point. Friction surfacing is a practicable method for the surface treatment of aluminum components in the transport industry, including marine, automotive and

* Corresponding author
E-mail address: moradi.malayeru@gmail.com (M. Moradi)

aviation. This process can be used for coating substrate metal to amend wear and corrosion resistance of the substrate. In addition, it is usually costly to design the whole components with aluminum alloys which have better wear and corrosion resistance. A high quality coating can improve the tribological properties of aluminium components. In order to obtain high quality coating, it is of great importance to select appropriate input parameters in friction surfacing. The trial and error method is time-consuming and cannot guarantee an optimal solution to improve coating qualities. In addition, it does not consider the interaction effects of the parameters. Design of experiments (DOE) has recently received great attention in various applications [2, 3] and Response surface methodology (RSM) is acknowledged as one of the DOE methods. RSM has been used in many manufacturing processes (i.e. welding, brazing, drilling, cutting and many others) but has not been used in Friction Surfacing before, as thoroughly as in this study. In the RSM technique, not only are the effects of the main parameters investigated, but also the interaction effects of the input parameters on responses can be considered.

According to literature review, Vitanov et al. [4] confirmed that RSM is an effective instrument to identify and develop significant relationships between the input and output parameters of the friction surfacing process. The authors identified that the velocity ratio is the most important parameter among the output parameters. In addition, the results indicated that the low to middle levels of the rotational speed and middle to high levels of the velocity ratio lead to the high quality of coating. Sugandhi and Ravishankar [5] developed empirical relationships via RSM to predict the coating width and coating thickness of the friction surfaced materials. The optimization process was carried out to attain the minimum thickness and maximum width. The developed empirical relationships could be efficiently used to estimate the influences of the process parameters on coating width and thickness. Sakihama et al. [6] examined the effects of the rotational speed, friction pressure, and traverse speed on some characteristics of the 5052 aluminum alloy friction surfaced deposits. Effects of the surfacing conditions on the thickness of the deposits, their surfacing efficiency, and microstructure were investigated. Moreover, the results of the tensile strength tests indicated that increasing the rotational speed and traverse speed of the consumable rod increases the tensile strength slightly; however, increasing the friction pressure decreases the tensile strength slightly. In this experiment, the highest tensile strength was 88.8% of that of the substrate. Tokisue et al. [7] carried out both the monolayer and multilayer friction surfacing to investigate the effects of the surfacing conditions on the microstructure and mechanical properties of the specimens. The 2017 aluminum alloy rod was used as the deposited material and the 5052 aluminum alloy was utilized as the substrate. Circular patterns were observed on the surfaces of both monolayer and multilayer deposits because of the rotating rod. The microstructure of the deposits and the deposition efficiency in both conditions were inspected. The results denoted that the multilayer surfacing has a higher deposition efficiency than the monolayer surfacing. In addition, the multilayer friction surfacing procedure brings on higher tensile strength than the monolayer friction surfacing procedure. Gandra et al. [8] employed the friction surfacing process to deposit AA6082-T6 on AA2024-T3 in order to investigate the mechanical characteristics of the coated specimens. Researchers also evaluated the thermo-mechanical transformations of the materials during the coating process. The obtained coatings demonstrated a thorough bonding without any porosity at the interface. However, the ultimate tensile strength of the coated samples was 25 % lower than that of the substrate. In addition, some delamination edges were observed in the coated samples. Friction surfacing was utilized to deposit H13 tool steel on low carbon steel by Rafi et al. [9]. Sound metallurgical bonding without any defects was observed on the substrates. The authors claimed that the influences of the plastic deformation and temperature lead to dynamic recrystallization and therefore fine-grained coating with no carbide particles. Moreover, Vickers micro-hardness profile across the coating/substrate interface indicated that the hardness of the coated sample was far more than that of the steel substrate. Nakama [10] investigated the friction surfacing of AZ91 magnesium alloy on AZ31 magnesium alloy using the monolayer procedure. The

shape and microstructure of the deposits were observed under different conditions. Moreover, temperature histories at different points were measured by thermocouples. Furthermore, hardness tests were conducted to unveil hardness distribution on the deposit and wear tests were carried out to compare the characteristics of the deposit and substrate. The deposit depicted higher hardness and wear resistance than the AZ31 magnesium alloy substrate. The mass transfer rate and specific energy consumption were quantified in the friction surfacing of mild steel by Gandra et al. [11]. This study represented a comprehensive investigation of different process parameters in the two categories of metallurgical and performance analyses. In addition, this research considered the effects of the tilt angle on metallurgical and performance analyses. Results indicated that the significant process parameter to amend joining efficiency and boost the deposition rate was the forging force. Rafi et al. [12] used H13 tool steel as the consumable rod and low carbon steel as the substrate in the friction surfacing process in order to investigate the effects of the rotational speed and traverse speed on coating shape, microstructure, and hardness. In addition, shear tests and bend tests were carried out to evaluate the mechanical properties of the coated specimens. The authors declared that the rotational speed is the most significant parameter influencing coating width, while coating thickness is mainly dependent on the traverse speed. Moreover, wider coating was achieved by lower rotational speed. The thinner coating which could be produced by higher traverse speed represented higher bond strength. In another study, Rafi et al. [13] investigated the friction surfacing of AISI 310 austenitic stainless steel on low carbon steel. The shape and microstructure of the deposits were observed to evaluate the influences of the traverse speed. The shear tests were conducted according to ASTM A264 to reveal interfacial bond strength and the three-point bending tests were carried out to determine the ductility of the coated specimens. In the experiments, the rotational speed and axial force were fixed. The results represented an austenitic structure without any cracks in the specimens. Besides, the implementation of lower traverse speeds leads to longer heating time and therefore wider heat affected zone (HAZ).

In the present research, the effects of three input parameters on dimensions, mechanical properties and microstructure of coating on the friction surfacing of Al7075-T6 over Al2024-T351 are inspected by the statistical approach. The input parameters are the rotational speed (1200 – 1600 rpm), axial force (3.14 – 6.28kN) and feed rate (100 – 300 mm/min). The coating width (w), coating thickness (t), ultimate tensile strength (S_u), and grain size of coating (GS_c) are considered as the output responses. Mechanical properties and microstructure of the specimens are studied to characterize coating properties. To amend coating properties mechanically and dimensionally, the input parameters are optimized and the optimized parameters are validated by an empirical experiment.

2. Design of Experiments

Response surface methodology (RSM) is a systematized and planned method to ascertain the relationships between the input factors influencing a process and the output responses [14]. The main advantages of the implementation of RSM are the identification of the principal factors having an impact on the friction surfacing process and the improvement of coating qualities. The objective is to find a functional relationship between the input and output parameters with a minimum error in the form of a mathematical model. A functional relationship relating a response η to the k levels of controlled variables can be expressed by Eq. (1) [15, 16]:

$$\eta = f(x1, x2, \ldots, xk) + \varepsilon \quad (1)$$

Where ε represents the random experimental error due to some unknown or uncontrollable variables. To optimize the response η, it is necessary to develop a suitable approximation for the functional relationships between the independent and response variables [17, 18]. The second order polynomial equation is used for representing the response and is also expressed in the form of Eq. (2):

$$\eta = \beta_0 + \sum_{i=1}^{k} \beta_i x_i + \sum_{i=1}^{k} \beta_{ii} x_i^2 + \sum_{i,j=1} \sum_{i<j} \beta_{ij} x_i x_j \quad (2)$$

Polynomial models are generally applicable for a relatively small area of the independent variables. In the current research, RSM is exploited to conduct a statistical analysis of the coating process by the friction surfacing. Three parameters, including the rotational speed, axial force, and feed rate are considered as input variables at three levels as shown in Table 1. Primary experiments are carried out by varying one variable while keeping other variables constant to determine the appropriate range of the input parameters. Therefore, the bonding interface characteristics are observed to determine the practical levels of the input parameters. The three-level central composite design is selected to run the experiments. It is composed of a core factorial that forms a cube with sides that are two-coded units in length (from -1 to +1 as noted in Table 1). The designed experiments and results of the experiments are reported in Table 2. The RSM analysis is carried out by Design-Expert V8 software. The software offers comprehensive descriptive statistics.

Table 1. Process input variables and levels

Variable	Symbol	Unit	Levels		
			-1	0	1
Axial Force	AF	N	3.14	4.71	6.28
Rotational Speed	RS	rpm	1200	1600	2000
Feed Rate	FR	mm/min	100	200	300

3. Experimental Set-up

To set up the experiments, a 2024-T351 aluminum plate is prepared as the substrate with dimensions 50 × 150 × 5 mm, and a 7075-T6 aluminum bar 20 mm in diameter and 100 mm in length is produced as the consumable rod. The chemical composition (the average of three XRF quantimeter measurements) and the mechanical properties of metals are reported in Table 3 and 4, respectively. The substrate is clamped on the table of a milling machine and the consumable rod is fixed in the vertical head of the machine for the friction surfacing of the specimens as shown in Fig. 1. The trial and error primary tests of the Friction Surfacing were conducted by varying one of the process variables to determine the effective range of each input parameter. Melting the rod material, smooth and uniform coating surface, absence of visible defects were the criteria used for selecting the suitable ranges. Therefore, based on our previous experimental studies and other researches' results, the level of the input parameters is considered in Table 1.

Table 3. Chemical compositions of materials (mass %).

Material	Cu	Mg	Mn	Fe	Cr	Si	Ti	Zn	Al
Plate	4.3	2.1	0.6	0.5	0.1	0.5	0.15	0.25	Bal.
Rod	1.7	2.4	0.08	0.1	0.2	0.04	0.15	5.6	Bal.

Table 2. Matrix design and measured results

Run	**Input Variables**			**Output Responses**			
	Axial Force (AF)	Rotational Speed (RS)	Feed Rate (FR)	Coating Width (mm)	Coating Thickness (mm)	Ultimate Tensile Strength(MPa)	Coating Grain Size (μm)
1	1	-1	-1	14	1.8	350	4
2	-1	-1	-1	22	3	390	3.5
3	0	0	1	25	0.7	410	3.3
4	-1	1	-1	21	0.9	420	4
5	1	1	1	21	0.5	375	4.7
6	-1	-1	1	24	1.5	405	2.8
7	0	0	0	21	0.95	410	2.8
8	0	-1	0	23	1.6	460	2.8
9	1	1	-1	20.5	0.9	350	2.8
10	0	0	0	21	0.7	415	2.8
11	0	0	-1	21.5	1.3	395	2.8
12	1	0	0	22	0.86	365	2.8
13	0	1	0	25	0.6	430	2.8
14	-1	0	0	21.5	1.4	360	3.5
15	1	-1	1	24	1.1	410	4.7
16	0	0	0	21	0.75	420	3.3
17	-1	1	1	20	1	400	2.8

Table 4. Mechanical properties of materials.

Material	Elongation (%)	Tensile strength (MPa)	Hardness (HV)
Plate	19	480	120
Rod	11	570	150

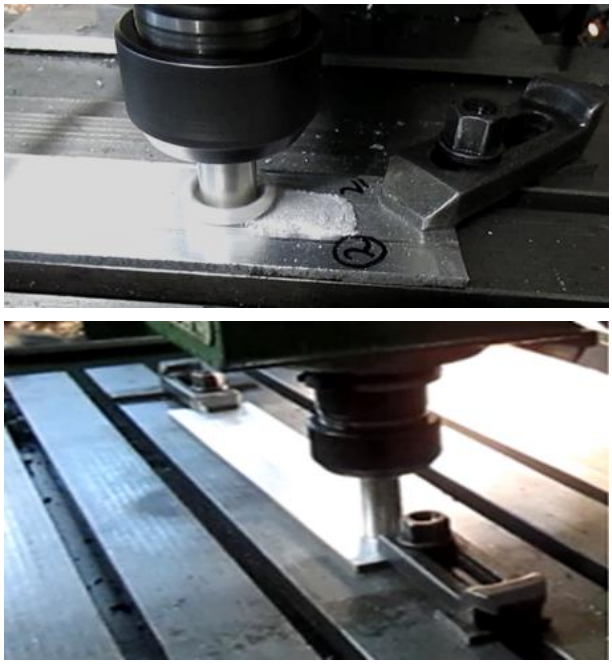

Fig. 1. Friction surfacing process (a) clamping the substrate on the table (b) consumable rod fixed inside the vertical head.

Figure 2 illustrates the coated specimen and coating dimensions such as width (w) and thickness (t) of the coating. Following the friction surfacing process, polishing operation was performed by TEGRA FORCE-5. In addition, the etching process in Graff - Sargent solutions (15.5 ml HNO_3, 3 gr CrO_3, 0.5 ml HF (48%), 84 ml H_2O) and Cl (2 ml HF, 5 ml HNO_3, 3 ml HCl, 190 ml H_2O) was accomplished each with a duration of 5 and 10 s. Finally, the specimens were examined by reflected light microscopy (ICM 405), and the images of the specimens were acquired in different magnifications. Furthermore, the grain size of the coating and that of the consumable rod were compared. Specimens were machined to run the tensile test according to standard ASTM-E8M with a cross-head speed of 2 mm/min at room temperature as shown in Fig. 3. The tensile strength tests were conducted by the INSTRON 5581 machine with 50 kN capacity. As it is depicted in Fig. 3(c) the axis of the tensile test was paralel to the direction of the coating.

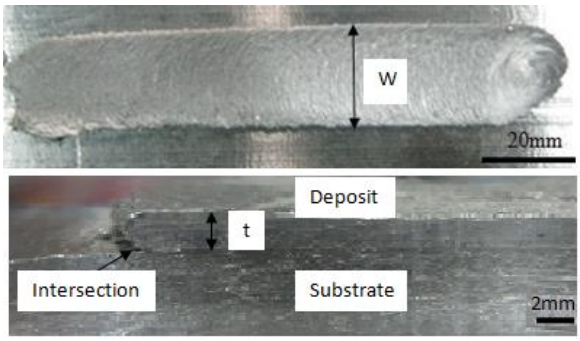

Fig. 2. Geometrical Dimensions of the deposit on the coated specimen.

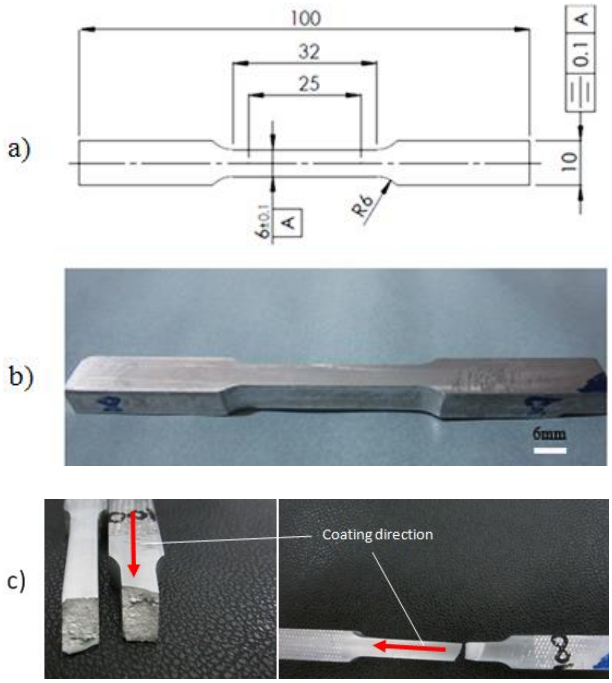

Fig. 3. Tensile test specimen according to standard ASTM-E8M a) dimensions of the specimen (in millimeters) b) machined tensile specimen c) coating direction on the tested specimen.

4. Results and Discussion

Coating width (w), coating thickness (t), ultimate tensile strength (S_u), and coating grain size (GS_c) were investigated as the output parameters of the friction surfacing process. RSM produces a mathematical model that can be used to predict a response. Analysis of variance (ANOVA), perturbation plots, and 3D surface plots are wide-ranging results to interpret data, identify significant input parameters, and assess the interaction effects of the parameters.

4. 1. Coating Width

Table 5 demonstrates the ANOVA analysis for coating width. The ANOVA table reveals that the axial force is the most important controlled variable for the width of coating. There are also significant interactions between the input parameters as ANOVA table shows. The difference between the predicted R-Squared and adjusted R-squared indicates that whether the model can be reliably used to interpolate the data. If the difference is less than 0.2, then the model fits the data and can be used to interpolate them. The subtraction of the adjusted R-squared from the predicted R-Squared, in this case, is 0.142.

Equation (3) is the predictive model of coating width in terms of coded factors.

$$(\text{Coating Width})^{-0.92} = +0.057 - 4.524\text{ E-}003\ AF - 1.085\text{E-}003\ RS - 6.221\text{E-}004\ FR + 5.049\text{E-}003\ (AF)(RS) - 4.270\text{E-}003\ (AF)(FR) - 3.930\text{E-}003\ (RS)(FR) + 8.876\text{E-}004\ AF^2 + 4.117\text{E-}003\ FR^2 + 3.233\text{E-}003\ (AF)(RS)(FR) + 4.195\text{E-}003\ AF^2FR \quad (3)$$

Equation (4) is thepredictive model of coating width in terms of actual factors:

$$(\text{Coating Width})^{-0.92} = - 0.048913 + 0.034840\ AF + 2.75569\text{E-}005\ RS + 8.79921\text{E-}004\ FR - 2.25473\text{E-}006\ (AF)(RS) - 2.69891\text{E-}004\ (AF)(FR) - 3.40702\text{E-}007(RS)(FR) - 3.04393\text{E-}003\ AF^2 + 4.11669\text{E-}007\ FR^2 + 5.14761\text{E-}008\ (AF)(RS)(FR) + 1.70200\text{E-}005\ AF^2FR \quad (4)$$

Coding reduces the range of each factor to a common scale, -1 to +1, regardless of their relative magnitude. The coded equation is also rewarding to ascertain the relative significance of the factors by comparing factor coefficients. The interaction terms in the predictive models imply that coating width is greatly dependent on all controlled factors. Fig. 4 illustrates the perturbation plot of coating width, which helps to compare the effects of all the factors on the central point in the design space. Coating width is plotted by changing only one factor over its range while holding the other factor constant. A steep slope or curvature in the factor shows that the response is sensitive to that factor. The perturbation plot indicates that increasing the axial force while holding the other factors constant results in the increase of coating width. There is also a similar trend in the rotational speed; however, increasing the rotational speed has less influence on coating width. Besides, the perturbation plot indicates that there is a maximum point for coating width exactly at the central point of the feed rate. Fig. 5(a) demonstrates the effects of the rotational speed and axial force on coating width in a 3D surface plot. It suggests that increasing the axial force at a lower rotational speed leads to a wider coating. It can be inferred that increasing the axial force and decreasing the rotational speed lead to higher friction and heat input, which, in turn, result in more plasticized materials. Therefore, the material deposit has wider width on the substrate. However, increasing the axial force at a higher rotational speed results in a narrower coating. Fig. 5(b) discloses the 3D surface plot of coating width in terms of the feed rate and axial force. The 3D surface plot of coating width in terms of the rotational speed and feed rate is shown in Fig 5(c).

Table 5. Analysis of variance (ANOVA) for coating width

Source	Sum of Squares	Degree of freedom (Df)	Mean Square	F Value	p-value Probe > F
Model	9.649E-004	10	9.649E-005	6.42	0.0168
Axial Force(AF)	2.047E-004	1	2.047E-004	13.63	0.0102
Rotational Speed(RS)	1.177E-005	1	1.177E-005	0.78	0.4101
Feed Rate(FR)	7.740E-007	1	7.740E-007	0.52	0.8280
(AF)(RS)	2.040E-004	1	2.040E-004	13.58	0.0103
(AF)(FR)	1.459E-004	1	1.459E-004	9.71	0.0285
(RS)(FR)	1.236E-004	1	1.236E-004	8.23	0.7040
AF^2	2.386E-006	1	2.386E-006	0.16	0.0918
FR^2	5.133E-005	1	5.133E-005	3.42	0.1140
(AF)(RS)(FR)	8.360E-005	1	8.360E-005	5.57	0.0564
AF^2FR	2.816E-005	1	2.816E-005	187	0.2200
Residual	9.013E-005	6	1.502E-005		
Lack of Fit	9.013E-005	4	2.253E-005	5.04	
Pure Error	0.000	2	0.000		
Cor Total	1.055E-003	16			
	Adj R-Squared	0.7722	R-Squared	0.9146	

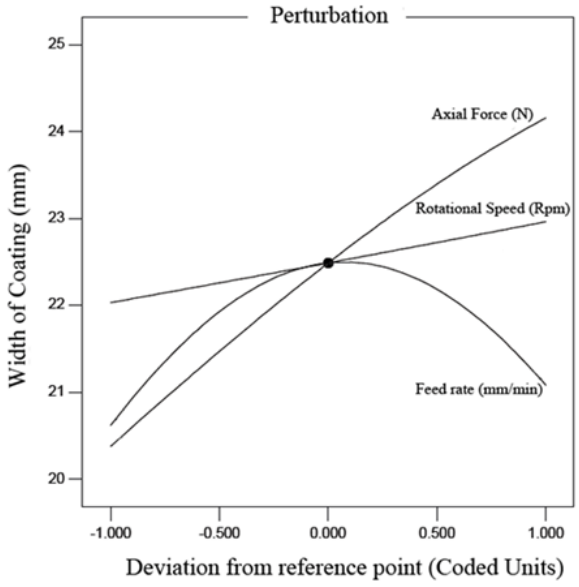

Fig. 4. Perturbation plot of coating width.

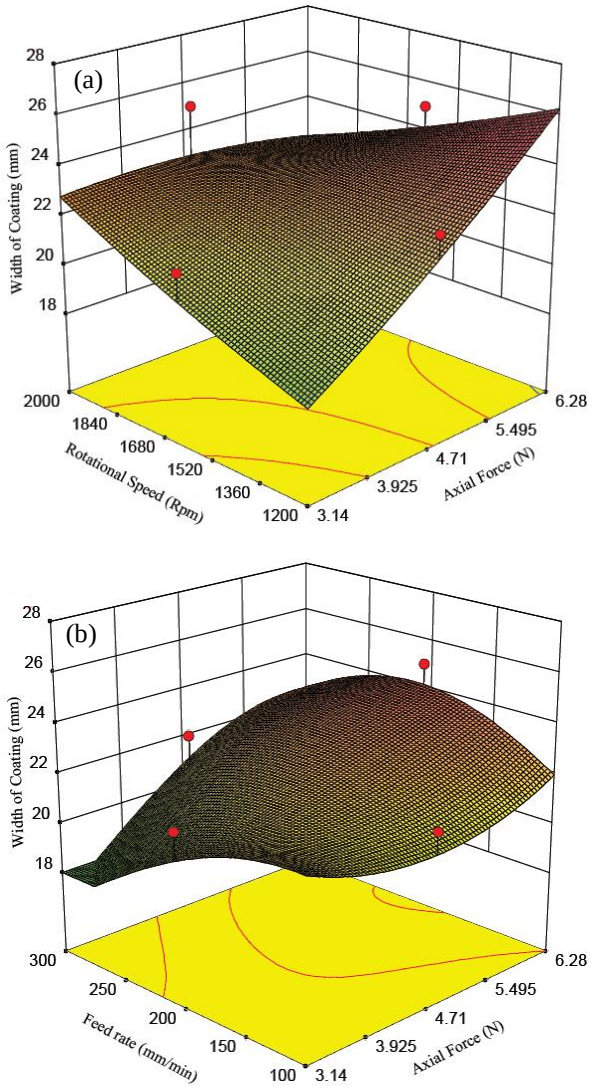

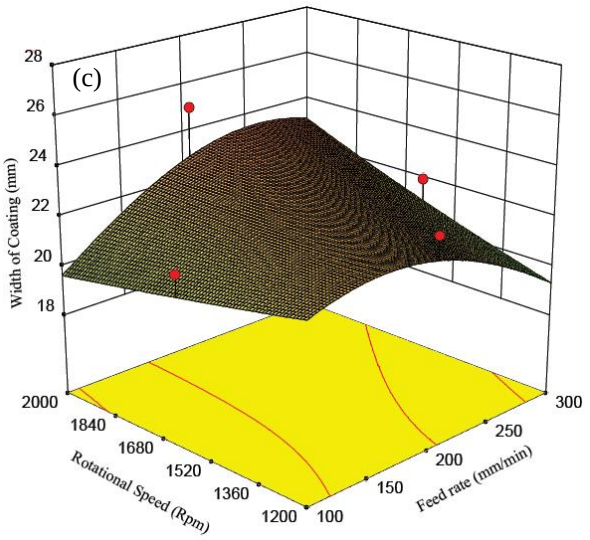

Fig. 5. 3D surface plots of coating width in terms of input variables.

4.2. Coating thickness

The ANOVA table reveals that the rotational speed is the most significant controlled variable regarding the thickness of coating. The axial force and feed rate also bring about important effects on coating thickness. Table 6 demonstrates the ANOVA analysis for coating thickness. The difference between the predicted R-squared and adjusted R-squared is 0.039 which asserts that the model can be effectively used to interpolate data.

Equation (5) is the predictive model of coating thickness in terms of coded factors:

$$(\text{Coating Thickness})^{0.14} = + 0.98 - 0.033\ AF - 0.058\ RS - 0.029\ FR + 0.015\ (AF)(RS) + 0.038\ FR^2 \quad (5)$$

Equation (6) is the predictive model of coating thickness in terms of actual factors:

$$(\text{Coating Thickness})^{0.14} = + 1.70275 - 0.058249\ AF - 2.55354E\text{-}004\ RS - 1.81995E\text{-}003\ FR + 2.32879E\text{-}005\ (AF)(RS) + 3.83217E\text{-}006\ FR^2 \quad (6)$$

Figure 6 illustrates the perturbation plot of coating thickness. The perturbation plot shows how increasing the rotational speed while holding the other factors constant results in the reduction of coating thickness. There is also a similar trend in the axial force. The perturbation plot shows that there is a minimum point for coating thickness close to the central point of the feed rate.

Table 6. Analysis of variance (ANOVA) for coating thickness

Source	Sum of Squares	Degree of freedom (Df)	Mean Square	F Value	p-value Probe > F
Model	0.061	5	0.012	23.07	<0.0001
Axial Force(AF)	0.011	1	0.011	20.59	0.0008
Rotational Speed(RS)	0.034	1	0.034	64.39	<0.0001
Feed Rate(FR)	8.241E-003	1	8.241E-003	15.63	0.0023
(AF)(RS)	1.711E-003	1	1.711E-003	3.25	0.0991
FR^2	6.047E-003	1	6.047E-003	11.47	0.0061
Residual	5.800E-003	11	5.272E-004		
Lack of Fit	4.847E-003	9	5.386E-004	1.13	0.5538
Pure Error	9.522E-004	2	4.761E-004		
Cor Total	0.067	16			
	Adj R-Squared	0.8733	R-Squared	0.9129	

The trivial difference between the predicted R-squared and adjusted R-squared affirms that the 3D surface plots, acquired from interpolation, are perfectly reliable. Fig. 7(a) demonstrates the effects of the axial force and rotational speed on coating thickness in a 3D surface plot. Although heat input increases while applying a greater axial force, it seems that increasing the rotational speed and axial force leads to less material deposition, which makes lower thickness while bonding the consumable rod on the substrates. This less material deposition might be the result of FR^2 parameter which has a high F-Value indicating that the feed rate has a remarkable influence on material deposition and consequently the thickness of coating. Fig. 7(b) illustrates the 3D surface plot of coating thickness in terms of the axial force and feed rate. 3D surface plot of coating thickness in terms of the rotational speed and feed rate is depicted in Fig 7(c).

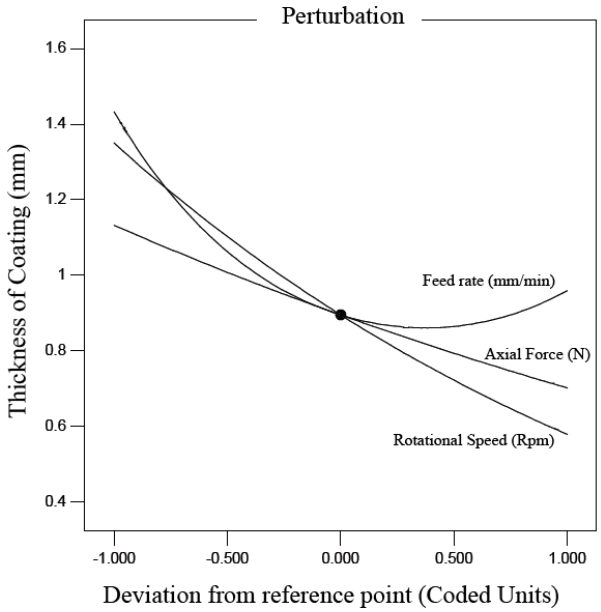

Fig. 6. Perturbation plot of coating thickness.

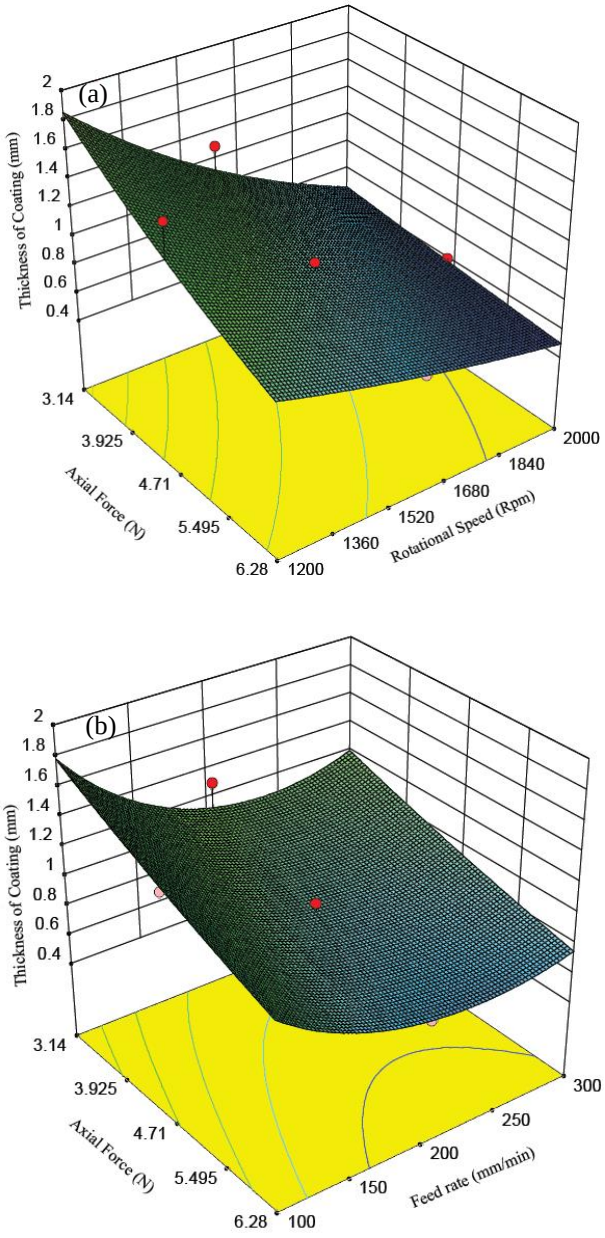

Fig. 7. 3D surface plots of coating thickness in terms of input variables.

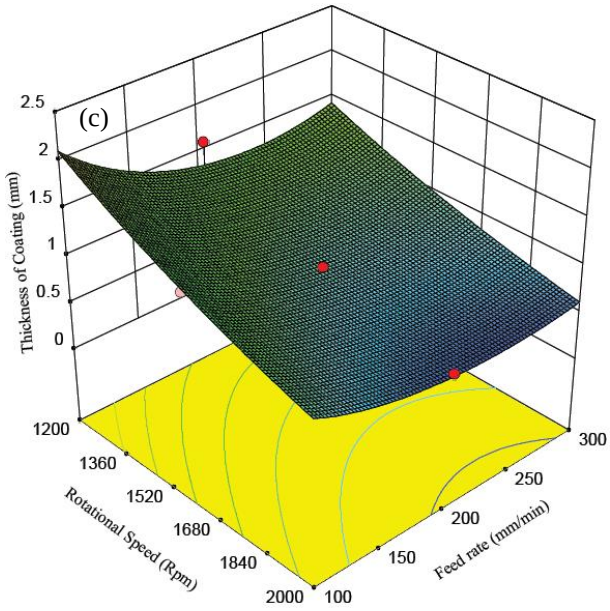

Fig. 7. Continue

4. 3. Ultimate tensile strength (S_u)

The ANOVA table reveals that the feed rate and axial force are the most significant controlled variables for the ultimate tensile strength. Rotational speed has almost no effect on the ultimate tensile strength. Table 7 demonstrates the ANOVA analysis for the ultimate tensile strength. The difference between the predicted R-squared and adjusted R-squared is 0.082 which affirms that the model can be used to interpolate data.

Equation (7) is the predictive model of the ultimate tensile strength in terms of coded factors:

$$(\text{Ultimate Tensile Strength})^{-0.76} = +0.010 - 2.133\text{E-}004\ AF + 7.342\text{E-}005\ RS + 2.742\text{E-}004\ FR + 1.765\text{E-}004\ (AF)(RS) - 2.495\text{E-}004\ (AF)(FR) - 5.722\text{E-}004\ RS^2 + 1.058\text{E-}003\ FR^2 \quad (7)$$

Equation (8) is the predictive model of the ultimate tensile strength in terms of actual factors:

$$(\text{Ultimate Tensile Strength})^{-0.76} = +5.82037\text{E-}003 - 2.67754\text{E-}004\ AF + 1.03045\text{E-}005\ RS - 3.21065\text{E-}005\ FR + 2.81047\text{E-}007\ (AF)(RS) - 1.58891\text{E-}006\ (AF)(FR) - 3.57647\text{E-}009\ RS^2 + 1.05830\text{E-}007\ FR^2 \quad (8)$$

Figure 8 depicts a typical stress-strain diagram of the experimental tensile tests of the coated sample #9. Fig. 9 illustrates the perturbation plot of the ultimate tensile strength. The perturbation plot shows that increasing the axial force while holding the other factors constant results in the increase of the ultimate tensile strength. Moreover, there is a minimum point for the ultimate tensile strength close to the central point of the rotational speed and there is a maximum point for the ultimate tensile strength close to the central point of the feed rate.

The processing temperature and material flow are two major parameters manipulating recrystallization. Microstructure evolutions (such as dynamic recrystallization) occur due to deformation at high temperature. By increasing the axial force, the material flow and consequently the strain increase, which leads to dynamic recrystallization and the structure becomes fine-grained so the ultimate tensile strength increases slightly.

Table 7. Analysis of variance (ANOVA) for the ultimate tensile strength

Source	Sum of Squares	Degree of freedom (Df)	Mean Square	F Value	p-value Probe > F
Model	5.403E-006	7	7.718E-007	10.78	0.0010
Axial Force(AF)	4.550E-007	1	4.550E-007	6.35	0.0327
Rotational Speed(RS)	5.390E-008	1	5.390E-008	0.75	0.4082
Feed Rate(FR)	7.518E-007	1	7.518E-007	10.50	0.0102
(AF)(RS)	2.492E-007	1	2.492E-007	3.48	0.0950
(AF)(FR)	4.978E-007	1	4.978E-007	6.95	0.0271
RS^2	9.917E-007	1	9.917E-007	13.85	0.0048
FR^2	3.392E-006	1	3.392E-006	47.37	<0.0001
Residual	6.445E-007	9	7.161E-008		
Lack of Fit	6.269E-007	7	8.956E-008	10.19	0.0923
Pure Error	1.759E-008	2	8.793E-009		
Cor Total	6.047E-003	16			
	Adj R-Squared	0.8105	R-Squared	0.8934	

As the rotational speed increases, the temperature goes up and it results in the loss of T6 heat treatment in the consumable rod and thus the strength is reduced. However, dynamic recrystallization occurs by increasing the rotational speed again, and granulation becomes finer and subsequently the strength increases. Moreover, at low feed rates the temperature is very high because of the high heat input per millimetre so that recrystallization occurs. Grain growth also happens because the temperature is adequately high. Therefore, low strength is likely at low feed rates. By further increasing the feed rate, the temperature increases a little and recrystallization occurs correspondingly without any grain growth. Hence it is obvious that the strength increases. However, at very high feed rates the temperature decreases, so the reduction of the strength is anticipated.

Figure 10(a) demonstrates the effects of the rotational speed and axial force on the ultimate tensile strength in a 3D surface plot. Fig. 10(b) shows the 3D surface plot of the ultimate tensile strength in terms of the feed rate and axial force. 3D surface plot of the ultimate tensile strength in terms of the feed rate and rotational speed is shown in Fig. 10(c). Assessment of the 3D surface shows the interaction of the feed rate and rotational speed, creating a hyperbolic paraboloid surface for the ultimate tensile strength.

In addition, comparison of the ultimate tensile strength data of the specimens obtained from Table 2 and of the consumable rod reported in Table 4 indicates that the average ultimate tensile strength is %30 lower than that of the consumable rod. It can be explained by the fact that the heat generated at the tip of the rod leads to the loss of T6 (artificial temper aging), and therefore the strength reduces. Nevertheless, the ultimate tensile strength of the coated specimens is normally acceptable.

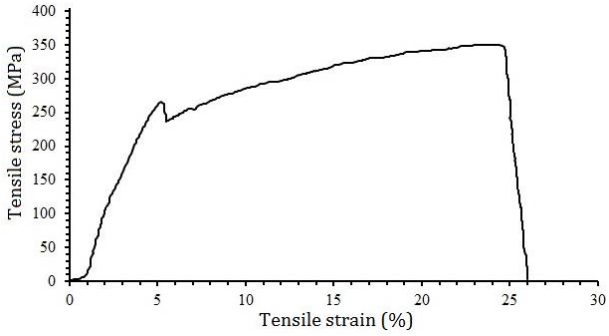

Fig. 8. A typical stress-strain diagram of the experimental tensile tests of the coated sample #9.

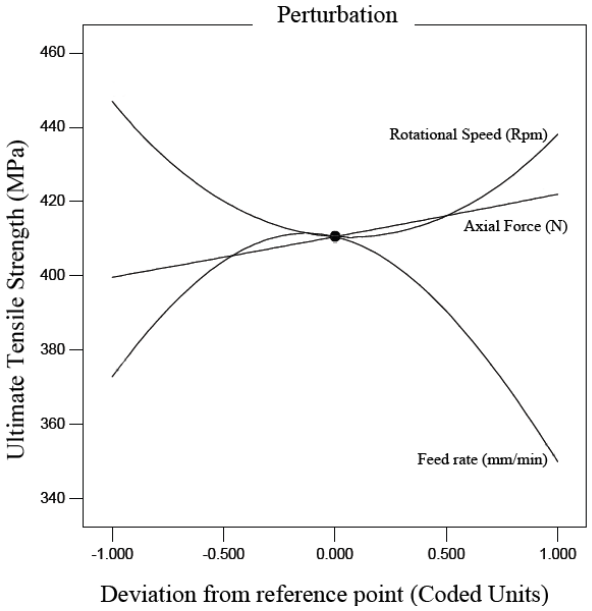

Fig. 9. Perturbation plot of the ultimate tensile strength.

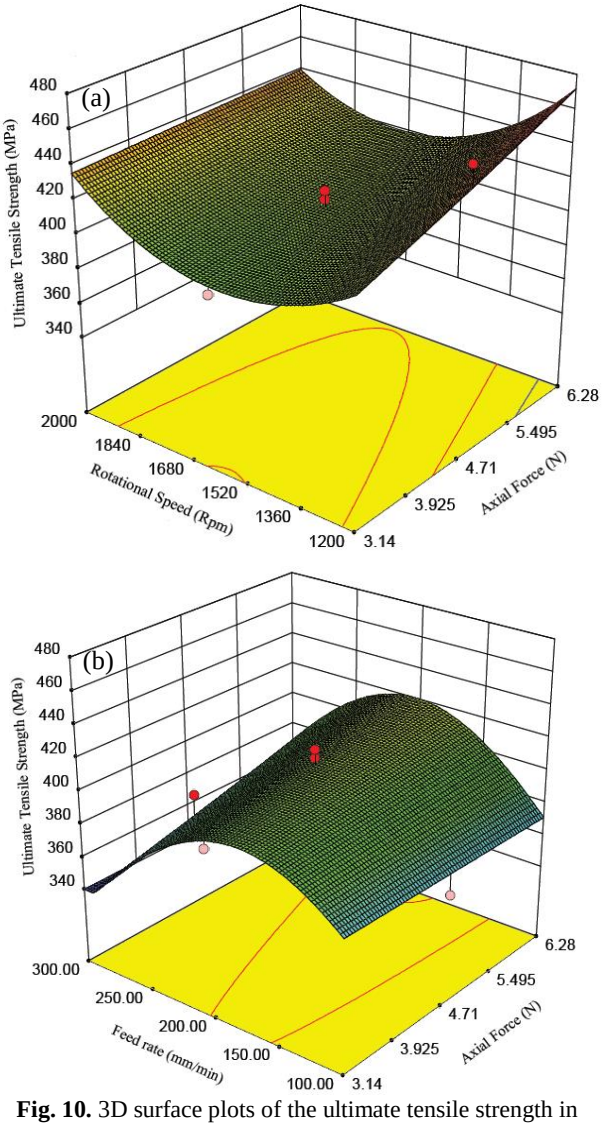

Fig. 10. 3D surface plots of the ultimate tensile strength in terms of input variables.

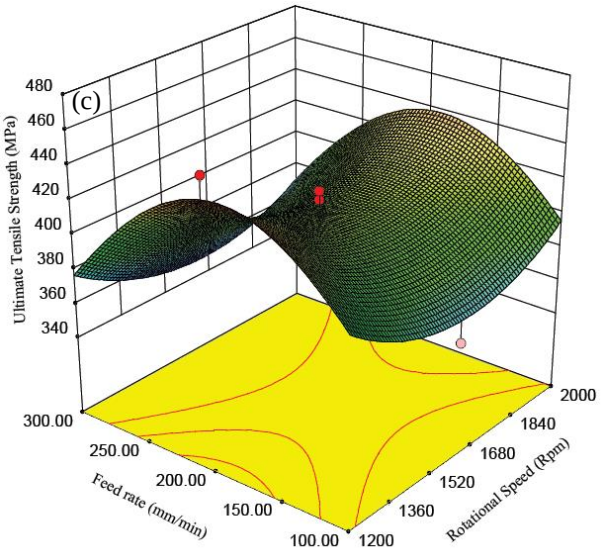

Fig. 10. Continue

4. 4. Coating grain size (GS_c)

The ANOVA table reveals that the interaction between the feed rate and axial force is the most significant controlled variable for coating grain size. Table 8 demonstrates the ANOVA analysis for coating grain size. The difference between the predicted R-Squared and adjusted R-squared is 0.093 that confirms the reliability of the model to interpolate data.

Equation (9) is the predictive model of coating grain size in terms of coded factors:

$$(\text{Coating Grain Size})^3 = +25.95 + 7.27\ AF + 12.19\ FR + 23.08\ (AF)(FR) + 24.97\ FR^2 \quad (9)$$

Equation (10) is the predictive model of coating grain size in terms of actual factors:

$$(\text{Coating Grain Size})^3 = +218.14561 - 24.77417\ AF - 1.56951\ FR + 0.14703\ (AF)(FR) + 2.49727E\text{-}003\ FR^2 \quad (10)$$

Figure 11 illustrates the perturbation plot of coating grain size. The perturbation plot reveals that the rotational speed has no effect on coating grain size, which also reconfirms the predictive model. Moreover, the plot shows that decreasing the axial force while keeping the feed rate constant results in the reduction of coating grain size; however, the changes in the feed rate cause a great deal of variation in coating grain size. By increasing the feed rate, recrystallization occurs because the temperature per millimeter unit decreases slightly, no grain growth occurs, and the structure becomes fine-grained.

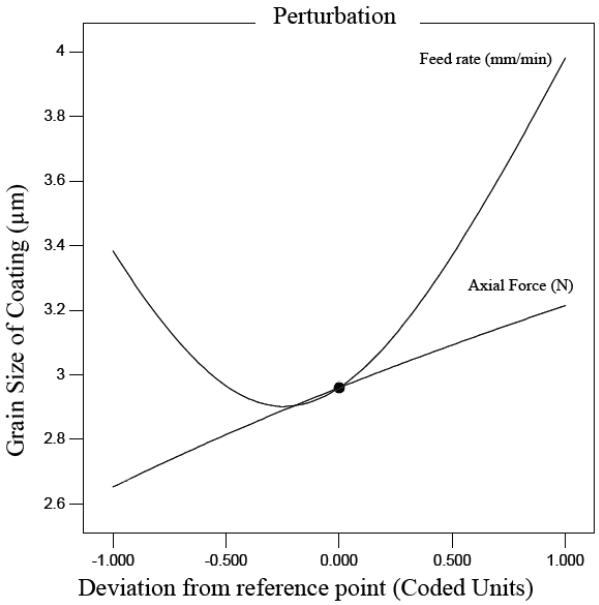

Fig. 11. Perturbation plot of coating grain size.

Table 8. Analysis of variance (ANOVA) for coating grain size

Source	Sum of Squares	Degree of freedom (Df)	Mean Square	F Value	p-value Probe > F
Model	8845.06	4	2211.27	7.74	0.0025
Axial Force(AF)	528.65	1	528.65	1.85	0.1987
Feed Rate(FR)	1485.86	1	1485.86	5.20	0.0416
(AF)(FR)	4262.65	1	4262.65	14.92	0.0023
FR^2	2567.91	1	2567.91	8.99	0.0111
Residual	3427.90	12	285.66		
Lack of Fit	2397.51	10	329.75	5.06	0.1763
Pure Error	130.39	2	65.19		
Cor Total	12272.96	16			
	Adj R-Squared	0.6276	R-Squared	0.7207	

Figure 12(a) demonstrates the effects of the feed rate and axial force on coating grain size in a 3D surface plot. Fig. 12(b) indicates the 3D surface plot of coating grain size in terms of the feed rate and rotational speed.

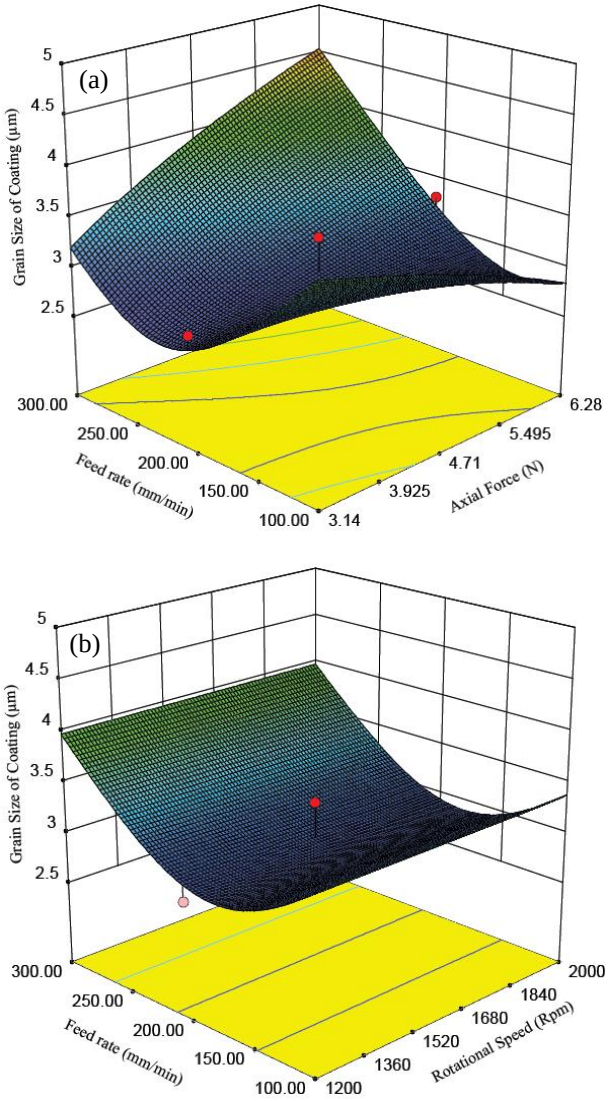

Fig. 12. 3D surface plots of coating grain size in terms of input variables.

Furthermore, the average grain size of the coated specimens obtained from the deposition process is almost 3.3µm as reported in Table 2, which shows about a 65% reduction compared to the grain size of the consumable rod (9.4 µm). Fig. 13 indicates that the coating grain size of a friction surfaced specimen is much finer and more homogeneous in comparison to that of the consumable rod and the substrate.

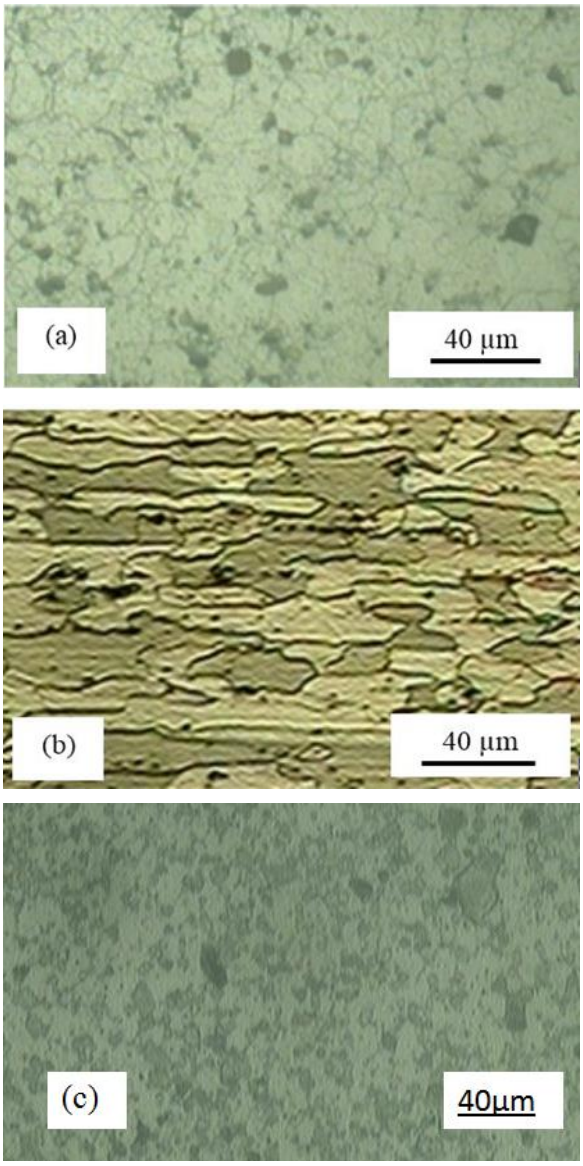

Fig. 13. The microstructure of the (a) consumable rod, (b) substrate, and (c) deposition (sample #8: Axial Force= 4.71 N, Rotational Speed= 1200 rpm, Feed Rate= 200 mm/min).

5-Numerical optimization

The optimization objective is to minimize coating grain size and maximize coating width, coating thickness, and the ultimate tensile strength. Smaller coating grain size leads to enhanced mechanical properties and homogenous bonding between the consumable rod and substrate. Moreover, wider coating area is desired to decrease the processing time of the friction surfacing. Additionally, thicker coating is advantageous to further withstand abrasion associated with mechanical erosion. Furthermore, the ultimate

tensile strength is a good indication of the mechanical performance of coating, which is considered to be higher. Table 9 shows the criterion for numerical optimization. The optimized process parameters to reach the optimization objective are shown in Table 10. Fig. 14 displays overlay plots which are comprised of yellow and grey contour plots obtained from each response being laid on top of the other. On each contour plot, the desirable area is yellow and the undesirable area is grayed-out. The remained yellow area for all responses defines the appropriate range of the input parameters. The optimized solution is implemented by a milling machine for coating the specimen to compare the experimental results and RSM predictions. Table 8 compares the characteristics of the optimized coated specimen with RSM predictions, which confirms that RSM predictions are fully in compliance with the experimental results. It should be noted that an error of about 10% in statistical analysis is an acceptable error and can be seen in many studies [19, 20].

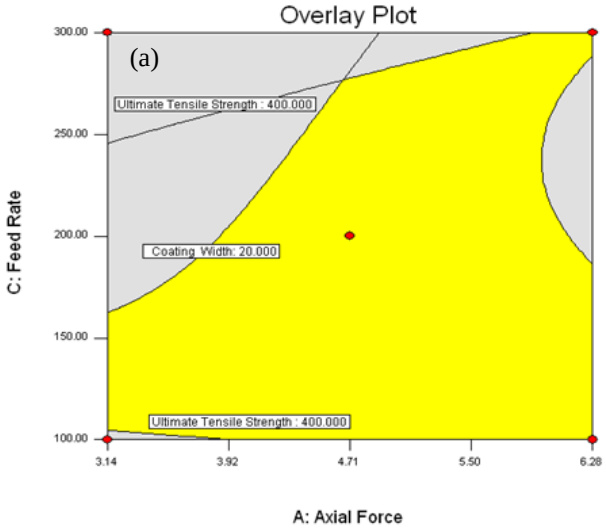

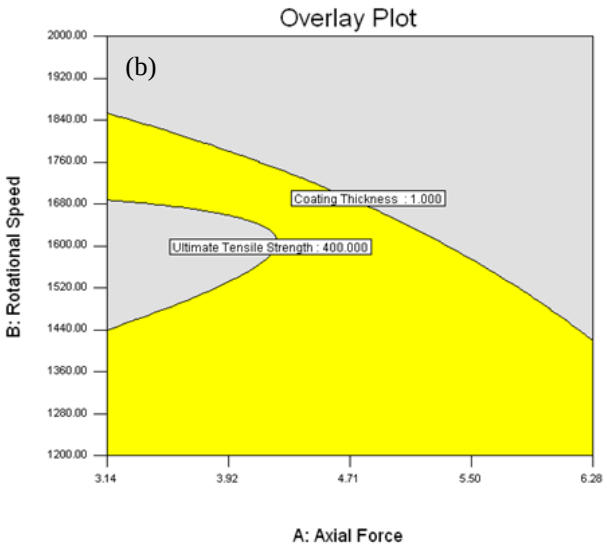

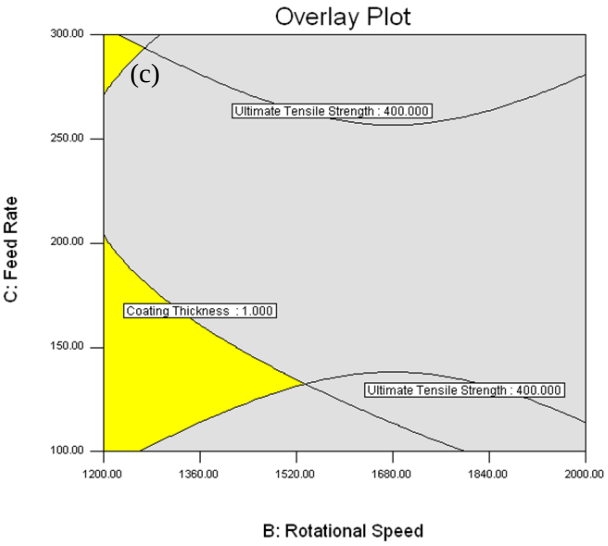

Fig. 14. Overlay plots in terms of the (a) feed rate and axial force (b) rotational speed and axial force (c) feed rate and rotational speed.

Table 9. Constraints and criteria of the input parameters and responses

Parameters/Responses		Name	Goal	Lower limit	Upper limit	Lower Weight	Upper Weight	Importance
Parameters		Axial Force	is in rang	3.14	6.28	1	1	-
		Rotational speed	is in rang	1200	2000	1	1	-
		Feed Rate	is in rang	100	300	1	1	-
Responses	Criteria	Coating Width	maximize	14	25	1	1	3
		Coating Thickness	maximize	0.5	3	1	1	3
		Ultimate Tensile Strength	maximize	350	460	1	1	3
		Coating Grain Size	minimize	2.8	4.7	1	1	3

Table 10 Predicted optimum results and experimental validation

Solution	Optimum input parameters			Desirability		Output responses			
	AF	RS	FR			Coating Width	Coating Thickness	Ultimate Tensile Strength	Coating Grain Size
					Actual	22.6	1.1	423	3.1
1	6.09	1200	143.31	0.717	Predicted	25	1.2322	449.012	2.7999
					Error%	-10.61%	-12.01%	-6.14%	9.68%

6. Conclusions

In the present research, the influences of three parameters, including the rotational speed, feed rate, and axial force, on the dimensions, mechanical properties and microstructure of friction surfaced AA7075-T6 coating over AA2024-T351 were investigated by the RSM methodology. Moreover, the optimal solution to attain high quality fine-grained homogeneous coating with larger dimensions was accomplished. The following results were obtained from this study:

1. Joining of two materials was achieved without any porosity at the interface of the two materials, and a fine-grained homogenous structure was attained.
2. Because of heat generation at the tip of the consumable rod during the process, T6 heat treatment was lost and the ultimate tensile strength of the deposition showed a 30% decrease compared to that of the consumable rod.
3. The deposited material had a fine-grained homogenous structure and the average grain size of the deposition was reduced by 65% compared to the rod.
4. Thickness of coating decreased by increasing the rotational speed, feed rate and axial force, and if the axial force was excessively high, it would bring about the development of a depression in the middle of the deposit.
5. Rotational speed had no effect on coating grain size, while decreasing the axial force resulted in the reduction of coating grain size.
6. The optimum process parameters for the friction surfacing of Al7075-T6 on Al2024-T351 are Axial Force= 6.09 (N), Rotational Speed= 1200 (rpm), and Feed Rate= 143.31(mm/min).
7. The overlay plots suggest that the ultimate tensile strength and coating thickness are the decisive responses to be considered to regulate the input parameters.

5. References

[1] H. Klopstock, A. R. Neelands, An improved method of joining or welding metals, British Patent specification (1941) 572789.

[2] M. Moradi, A. Mohazabpak, Statistical modelling and optimization of laser percussion micro-drilling on Inconel 718 sheet using response surface methodology (RSM), *Lasers in Engineering* 39 (4-6) (2018) 313-331.

[3] M. Azadi, S. Azadi, F. Zahedi, M. Moradi, Multidisciplinary optimization of a car component under NVH and weight constraints using RSM, ASME 2009 International Mechanical Engineering Congress and Exposition, 13-19 November 2009, Lake Buena Vista, Florida, USA. 15: Sound, *Vibration and Design* 315-319.

[4] V. I. Vitanov, N. Javaid, D. J. Stephenson, Application of response surface methodology for the optimisation of micro friction surfacing process, *Surface and Coatings Technology* 204(21) (2008) 3501-3508.

[5] V. Sugandhi, V. Ravishankar, Optimization of friction surfacing process parameters for aa1100 aluminum alloy coating with mild steel substrate using response surface methodology (RSM) technique, *Modern Applied Science* 6(2) (2012) 69-80.

[6] H. Sakihama, H. Tokisue, K. Katoh, Mechanical properties of friction surfaced 5052 aluminum alloy, *Materials Transactions* 44(12) (2003) 2688-2694.

[7] H. Tokisue, K. Katoh, T. Asahina, T. Usiyama, Mechanical properties of 5052/2017 dissimilar aluminum alloys deposit by friction surfacing, *Materials Transactions* 47(3) (2006) 874-882.

[8] J. Gandra, D. Pereira, R. M. Miranda, R. J. C. Silva, P. Vilaça, Deposition of AA6082-T6 over AA2024-T3 by friction surfacing-Mechanical and wear characterization, *Surface and Coatings Technology* 223 (2013) 32-40.

[9] H. K. Rafi, G. J. Ram, G. Phanikumar, K. P. Rao, Microstructural evolution during friction surfacing of tool steel H13, *Materials & Design* 32(1) (2011) 82-87.

[10] D. Nakama, K. Katoh, H. Tokisue, Some characteristics of AZ31/AZ91 dissimilar magnesium alloy deposit by friction surfacing, *Materials Transactions* 49(5) (2008) 1137-1141.

[11] J. Gandra, R. M. Miranda, P. Vilaça, Performance analysis of friction surfacing, *Journal of Materials Processing Technology* 212(8) (2012) 1676-1686.

[12] H. K. Rafi, G. J. Ram, G. Phanikumar, K. P. Rao, Friction surfaced tool steel (H13) coatings on low carbon steel: A study on the effects of process parameters on coating characteristics and integrity, *Surface and Coatings Technology* 205(1) (2010) 232-242.

[13] H. K. Rafi, G. J. Ram, G. Phanikumar, K. P. Rao, Friction surfacing of austenitic stainless steel on low carbon steel: Studies on the effects of traverse speed, *In Proceedings of the World Congress on Engineering* (Vol. 2) (2010).

[14] R. H. Meyers, D. C. Montgomery, Response surface methodology, Process and Product Optimisation Using Design Experiments, second ed. (2002) Willey, New York, NY.

[15] M. S. Meiabadi, A. Kazerooni, M. Moradi, Numerical analysis of laser assisted titanium to polyimide welding using statistical approach, *International Journal of Laser Science: Fundamental Theory and Analytical Methods* 1(2) (2018) 185-205.

[16] M. Moradi, H. Abdollahi, Statistical modelling and optimization of the laser percussion microdrilling of thin sheet stainless steel, *Journal of lasers in Engineering* 40 (4-6) (2018) 375-393.

[17] M. Moradi, O. Mehrabi, T. Azdast, Kh. Y. Benyounis, Enhancement of low power CO2 laser cutting process for injection molded polycarbonate, *Optics & Laser Technology* 96C (2017) 208–218.

[18] H. Abdollahi, R. Mahdavinejad, M. Ghambari, M. Moradi, Investigation of green properties of iron/jet-milled grey cast iron compacts by response surface method, *Proceedings of the Institution of Mechanical Engineers, Part B: Journal of Engineering Manufacture* 228(4) (2014) 493-503.

[19] M. Moradi, M. Karami Moghadam, High power diode laser surface hardening of AISI 4130; statistical modelling and optimization, *Optics & Laser Technology* 111 (2019) 554-570.

[20] M. S. Moradi, S. Meiabadi, A. Kaplan, 3D Printed Parts with Honeycomb Internal Pattern by Fused Deposition Modelling; Experimental Characterization and Production Optimization, *Metals and Materials International* 25 (5) (2019) 1312-1325.

بهینه سازی چندمنظوره خواص مکانیکی و متالورژیکی فرآیند پوشش دهی AL7075-T6 بر AL2024-T351 به روش پوشش دهی اصطکاکی با استفاده از روش RSM و تابع مطلوبیت کل

محمد مصطفی‌پور[۱]، محمود مرادی[۲]، حامد کمالی[۳]، محمد صالح میابادی[۴]، الکساندر کاپلان[۵]

۱- بخش مهندسی مکانیک، دانشکده مهندسی مکانیک، دانشگاه تبریز، تبریز، ایران.
۲- بخش مهندسی مکانیک، دانشکده مهندسی ، دانشگاه ملایر، ملایر، ایران.
۳- بخش مهندسی مکانیک، دانشکده مهندسی مکانیک، دانشگاه مراغه، مراغه، ایران.
۴- بخش مهندسی مکانیک، دانشگاه پلی‌تکنیک مونترال، مونترال، کانادا.
۵- بخش علوم مهندسی و ریاضیات، دانشگاه فنی لولئو، لولئو، سوئد.

چکیـــده

پوشش دهی نقشی اساسی در مهندسی سطح دارد، و منجر به ارتقا خواص مکانیکی و متالورژیکی تولیدات می شود. همچنین مزایای اقتصادی و صرفه جویی در هزینه ها در ارتقای خواص سطح قطعات را به همراه دارد. پوشش دهی اصطکاکی روشی نسبتا جدید برای ایجاد سطحی همگن، پوشش ریز دانه و مقاوم به سایش و خوردگی می باشد. در این تحقیق رسوب دهی AA7075-T6 بر روی زیرلایه AA2024-T351 مورد بررسی قرار گرفت. روش رویه پاسخ جهت بررسی تاثیر پارامترهای سرعت دورانی، نیروی عمودی، و نرخ پیشروی بر خواص مکانیکی و ریزساختاری نمونه ها استفاده گردید. عرض پوشش، ضخامت پوشش، استحکام کششی تسلیم، و اندازه دانه پوشش به عنوان پاسخ های فرآیند مطرح شدند. پارامترهای ورودی برای دستیابی به پهنا و ضخامت بیشتر پوشش با استحکام کششی بالاتر و دانه های ریزتر بهینه سازی شدند. نتایج حاکی از آن است که اتصال این دو ماده بدون هیچ گونه تخلخل در فصل مشترک یا محل اتصال دو ماده انجام پذیرفت. همچنین ریزساختاری ریزدانه و همگن در پوشش مشاهده گردید. میانگین اندازه دانه های پوشش تا ۶۵٪ اندازه دانه میله مصرفی کاهش داشته است.

واژه‌های کلیدی: پوشش دهی اصطکاکی، خواص مکانیکی، پوشش دهی آلومینیوم، بهینه سازی، طراحی آزمایش‌ها